Supporting Information

Strong Plasmon-Exciton Coupling in Bimetallic Nanoring and Nanocuboid

Na Li[1,‡], Zihong Han[1,‡], Yuming Huan[2,‡], Kun Liang[2,‡], Xiaofeng Wang[1], Fan Wu[2], Xiaoying Qi[1], Yingxu Shang[1], Li Yu[2] and Baoquan Ding[1,3,4,*]

[1]CAS Key Laboratory of Nanosystem and Hierarchical Fabrication, CAS Center for Excellence in Nanoscience, National Center for Nanoscience and Technology, 11 BeiYiTiao, ZhongGuanCun, Beijing 100190, China
[2]State Key Laboratory of Information Photonics and Optical Communications, Beijing University of Posts and Telecommunications, 10 Xitucheng Road, Beijing, 100876, China
[3]University of Chinese Academy of Sciences, Beijing 100049, China
[4]School of Materials Science and Engineering, Zhengzhou University, Zhengzhou 450001, China

E-mail: dingbq@nanoctr.cn
‡These authors contributed equally to this work.

Materials and Methods

Materials. H_2O_2 (30 wt %) was purchased from Aladdin. Acetonitrile was purchased from Fisher Chemical. Sodium citrate (SC), Silver nitrate ($AgNO_3$), Sodium borohydride ($NaBH_4$), L-ascorbic acid (AA), Hydroxylamine hydrochloride (Hya), sodium hydroxide (NaOH), hydrogen tetrachloroaurate (III) trihydrate ($HAuCl_4 \cdot 3H_2O$), bis(p-sulfonatophenyl)-phenylphosphine dihydrate dipotassium (BSPP), hexadecylpyridinium chloride monohydrate (CPC), 5,6-Dichloro-2-[[5,6-dichloro-1-ethyl-3-(4-sulfobutyl)-benzimidazol-2-ylidene]-propenyl]-1-ethyl-3-(4-sulfobutyl)-benzimidazolium hydroxide, inner salt (TDBC), Cetyltrimethyl Ammonium Bromide (CTAB) were purchased from Sigma-Aldrich. All chemicals were used as received without further purification. Ultrapure water obtained from a Milli-Q system was used in all experiments. All glassware was cleaned using freshly prepared aqua regia (HCl: HNO_3 in a 3:1 ratio by volume) and copious amounts of deionized water.

Synthesis of Au Nanorings. Au nanorings were fabricated through a template method by selective Au deposition on the edges of silver nanoplates and subsequent Ag etching, followed by a second Au deposition. Details are as follows:

Preparation of Ag Nanoplates. Ag nanoplates were prepared according to previous literature with some modification. First, Ag seeds were prepared as follows: To 200 mL of deionized water (DIW), aqueous solutions of sodium citrate (0.0045 M), silver nitrate (1×10^{-4} M), and 480 μL H_2O_2 (30 wt %) were added,

followed by adding an icecold, fresh prepared aqueous solution of sodium borohydride (0.1 M 1.2 mL) with vigorous stirring. After 5 min of stirring, the solution was left undisturbed for 2 h in 4 °C. The synthesized Ag nanoseeds were concentrated by centrifugation before use. Second, Ag nanoplates were prepared as follows: To 44 mL of deionized water (DIW), 20 mL of acetonitrile, 300 μL of ascorbic acid (0.1 M), 200 μL sodium citrate (0.075 M), and Ag seeds were added, followed by adding 240 μL of silver nitrate (0.1 M) with vigorous stirring for 30 min. The Ag nanoplates were centrifuged and washed with water for future use.

Preparation of Au Nanorings. Au nanorings were prepared according to previous literature with some modifications. First, Ag@Au nanoplates were prepared as follows: Basic hydroxylamine hydrochloride solution (3 mM) was prepared. The as-prepared Ag nanoplates were dissolved in 20 mL of water in a glass container placed in an ice bath. To this solution, the basic hydroxylamine hydrochloride and an aqueous solution of hydrogen tetrachloroaurate (III) trihydrate ($HAuCl_4 \cdot 3H_2O$, 0.3 mM) were added via syringe pump at a rate of 2 mL/h with vigorous stirring. After 30 mins, The Ag@Au nanoplates were centrifuged. Secondly, the thin Au nanorings were prepared as follows: The as-prepared Ag@Au nanoplates were incubated with 5 mL solution of bis (p-sulfonatophenyl)-phenylphosphine dihydrate dipotassium (BSPP, 2 mM) to etch the Ag templates. The reaction was monitored by UV-vis spectroscopy to indicate the completion of etching. The resulting thin Au nanorings were centrifuged. Finally, to prepare thicker Au nanorings, the thin Au nanorings were dispersed in 20 mL of water. The above basic hydroxylamine hydrochloride solution and aqueous solution of $HAuCl_4 \cdot 3H_2O$ were added via syringe pump at a rate of 2 mL/h with vigorous stirring. The reaction was monitored by UV-vis spectroscopy to determine the thickness of Au nanorings.

Synthesis of Au@Ag core-shell nanorings structure. In a typical method, 100 μL of the Au nanorings (0.5 nM) and 16 μL of CPC aqueous solution (0.1 M) were mixed together. Then, different amounts (2-15 μL) of $AgNO_3$ (10 mM) and 8 μL of AA (0.1 M) were added consecutively. The mixture was heated up to 60 °C for 1 h then cooled to room temperature. The as-synthesized Au@Ag nanorings were centrifuged at 5000 rpm for 3 min and resuspended in deionized water (DIW).

Preparation of Au@Ag nanorings/J-aggregate hybrids. We prepared monodisperse Au@Ag nanorings/J-aggregate hybrids based on the previous work with some modifications.[1-5] We directly coated CPC-stabilized Au@Ag nanorings with TDBC without supplementary addition of salts or bases during the

synthesis and carried out at room temperature. The fabrication of Au@Ag nanorings/J-aggregate hybrids based on electrostatic self-assembly. This simple preparation process is also reproducible allowing sufficient, high quality Au@Ag nanorings/J-aggregate hybrids to be made for photonic applications. The experimental details are attached below: The as-prepared Au@Ag nanorings were incubated with 5 μL of TDBC (5 mM) for 1 h. Then the resulting samples were centrifuged and washed twice with water.

Synthesis of Au Nanorods. The gold nanorods were synthesized via a seed-mediated growth method. The seed solution for Au nanorods was prepared as reported previously. A 5 mL amount of 0.5 mM $HAuCl_4$ was mixed with 5 mL of 0.2 M CTAB solution. A 0.6 mL portion of fresh 0.01 M $NaBH_4$ was diluted to 1 mL with water and was then injected into the Au (III)-CTAB solution under vigorous stirring (1200 rpm). The solution color changed from yellow to brownish-yellow, and the stirring was stopped after 2 min. The seed solution was aged at room temperature for 2 h before use. To prepare the growth solution, 0.9 g of CTAB together with 0.08 g of sodium salicylate were dissolved in 25 mL of warm water (70°C) in a 500 mL Erlenmeyer flask. The solution was allowed to cool to 30°C, then a 600 μL of 4 mM $AgNO_3$ solution was added. The mixture was kept undisturbed at 30 °C for 15 min, after which 25 mL of 1 mM $HAuCl_4$ solution was added. After 15 min of slow stirring (400 rpm), 1mL of 0.064 M ascorbic acid was added, and the solution was vigorously stirred for 30 s until it became colorless. Finally, 80 μL of seed solution was injected into the growth solution. The resultant mixture was stirred for 30 s and left undisturbed at 30 °C for 12 h for Au nanorods growth. The reaction products were isolated by centrifugation at 3000 rpm for 15 min followed by removal of the sediment to remove Au nanoparticles. And then the reaction products were isolated by centrifugation at 8500 rpm for 15 min followed by removal of the supernatant, and washed once with water.

Synthesis of Au@Ag core-shell nanocuboids structure. In a typical method, 100 μL of the Au nanorods (0.5 nM) and 16 μL of 0.1 M CPC aqueous solution were mixed together. Then, different amounts (0.5-5 μL) of 10 mM $AgNO_3$ and 8 μL of 0.1 M AA were added consecutively. The mixture was heated up to 60 °C for 1 h then cooled to room temperature. The as-synthesized Au@Ag nanocuboids were centrifuged at 8600 rpm for 3 min and re-suspended in deionized water (DIW).

Preparation of Au@Ag nanocuboids/J-aggregate complex. The as-prepared Au@Ag nanocuboids were incubated with 5 μL of TDBC (5 mM) for 1 h. Then the resulting samples were centrifuged and washed twice with water.

Optical characterization. Extinction spectra were measured using a Shimadzu UV-2450 UV-vis spectrophotometer. The scanning was carried out at a range of 230-900 nm at room temperature in a 1 cm-length cell and the scan rate was 300 nm/min.

TEM characterization. Before depositing the sample solution, the grids were first glow discharged using Emitech K100X machine in order to increase its hydrophilicity. The samples for TEM imaging were prepared by placing 5 μL of the sample solution on a carbon-coated copper grid (300 meshes, Ted Pella). After 10 min of deposition, the unbound sample was wicked away from the grid using filter paper. To remove the excess salt, the grid was touched with a drop of water, and the excess water was wicked away using filter paper. The grid was kept at room temperature to evaporate excess solution. TEM imaging was carried out using a Hitachi HT-7700, operated at 80 kV. The high resolution TEM (HRTEM) and energy dispersive X-ray spectroscopy mapping (EDX mapping) were conducted using a Tecnei G2-20S-TWIN system, operated at 200 kV.

SEM characterization. The SEM images were taken by Hitachi S-4800 (Japan) microscope operating at 10.0 kV.

Dark-filed scattering measurements. Before dark-filed scattering measurements, 5 μL of the Au@Ag nanoring/J-aggregate or Au@Ag nanocuboid/J-aggregate hybrids bulk solution was drop-casted onto ITO-coated glass substrate. After 3 min, the droplet were removed and washed with deionized water. Then, the samples were dried under nitrogen conditions and the single isolated Au@Ag nanoring/J-aggregate or Au@Ag nanocuboid/J-aggregate hybrids could be formed and fixed on the surface of ITO-coated glass substrate. The use of ITO substrates allows the Au@Ag nanoring/J-aggregate or Au@Ag nanocuboid/J-aggregate hybrids to be characterized with both SEM and dark-field imaging. To obtain the scattering spectroscopy of the individual hybrids, we combined dark-field spectroscopy with SEM of the same field of view to correlate elastic scattering spectra and structures on the level of single hybrid Au@Ag nanoring/J-aggregate or Au@Ag nanocuboid/J-aggregate. The hybrids were first characterized by optical spectroscopy and after by SEM to avoid any damages caused by the electron beam. The scattering images and spectra of the individual Au@Ag nanoring/J-aggregate or Au@Ag nanocuboid/J-aggregate were recorded on a dark-field optical microscope (Olympus BX51, Olympus Inc.) that was integrated with a quartz tungsten halogen lamp (100 W), a monochromator (Andor 303i, ANDOR Tec.), and a charge-coupled device camera (iXon Ultra 888, ANDOR Tec.). The camera was thermoelectrically cooled to -65

°C during the measurements. In order to obtain clean scattering signals from a single isolated hybrid, the commercial spectrograph equipped with an entrance slit was set at ~100 nm. For collection of the scattering spectra, the light was launched from a dark-field objective (100×, numerical aperture 0.80), and the light scattered in the backward direction was collected by the same objective. The scattering signals from the individual hybrids were corrected by first subtracting the background spectra taken from the adjacent regions without hybrids and then dividing them with the calibrated response curve of the entire optical system. Color scattering images were captured using a color digital camera (Retiga R3, Qimaging) mounted on the imaging plane of the microscope. To determine the plasmon resonance peak of the bear Au@Ag nanorings or Au@Ag nanocuboids (i.e., uncoupled Au@Ag nanorings or Au@Ag nanocuboids), we utilized the photobleaching method to destroyed the J-aggregate exciton systems covered around the hybrids by illuminating with a picosecond laser (PS-R-532, Changchun New Industries Optoelectronics Technology Co., Ltd.). After photobleaching treatment, Rayleigh scattering spectra of the uncoupled Au@Ag nanorings or Au@Ag nanocuboids were collected on the same dark-field scattering system.

Finite-difference time-domain (FDTD) simulation. Numerical simulations of Au@Ag nanoring and Au@Ag nanocuboid were performed using FDTD method. The material data of Au@Ag nanoring and Au@Ag nanocuboid were from Johnson and Christy.[6] Both of these structures were excited by a plane wave at normal incidence polarized along the longitudinal direction and the extinction spectra were calculated by using cross section tool. We also calculated the electric field distribution and mode volume to further explore the feature of our structures. The background index was set to 1.33. The dielectric function of J-aggregate was approximated by Lorentz model $\varepsilon(\omega) = \varepsilon_\infty + f \cdot \omega_0{}^2/(\omega_0{}^2 - i\Gamma_e\omega - \omega^2)$ with $\varepsilon_\infty = 2.1$, resonance $\omega_0 = 2.116$eV, linewidth $\gamma = 25$ meV. We used different oscillator strength f=0.075, 0.03 for ring and cuboid, respectively and the simulation fits our experimental result well.

Theory and equations of strong coupling. For a system of N quantum emitters (QEs) strongly interacting with a single metallic nanoparticle, the total coupling coefficient g is given by

$$g = \sqrt{N} g_0 \tag{1}$$

N is the number of QEs interacting with nanoparticle. g_0 is the coupling coefficient between a exciton and single metallic nanoparticle, which can be simply described by

$$g_0 = \mu_e \left| E_{vac} \right| = \mu_e \sqrt{\frac{\hbar\omega_0}{2\varepsilon\varepsilon_0 V}} \tag{2}$$

Here μ_e denotes the transition dipole moment and E_{vac} is the electric field intensity in vacuum field. V is the mode volume of electric field. Then we use coupled oscillator model to describe the strongly coupled exciton-plasmon hybrid system.

$$H = \hbar \begin{pmatrix} \omega_e & g \\ g & \omega_p \end{pmatrix} \tag{3}$$

where ω_e and ω_p are the resonance frequency of exciton and plasmon, respectively. $\hbar$ is the reduced Planck constant and set to 1. It is necessary to take the damping into account in an plasmonic nanocavity. So we define that $\tilde{\omega}_e = \omega_e - i\Gamma_e/2$ and $\tilde{\omega}_p = \omega_p - i\Gamma_p/2$, Γ_e and Γ_p are the line width of the transition of exciton and plasmon respectively, which represent the damping rate of exciton and plasmon. Then the Hamiltonian matrix of this coupled hybrid system can be given by

$$H = \begin{pmatrix} \omega_e - i\frac{\Gamma_e}{2} & g \\ g & \omega_p - i\frac{\Gamma_p}{2} \end{pmatrix} \tag{4}$$

From Eq. (4), we can obtain the energy eigenvalue, which is

$$\omega_{\pm} = \frac{\omega_e + \omega_p}{2} - i\frac{\Gamma_e + \Gamma_p}{4} \pm \frac{1}{2}\sqrt{4Ng_0^2 + (\Delta - i\frac{\Gamma_e - \Gamma_p}{2})^2} \tag{5}$$

$\Delta = \omega_e - \omega_p$ is the detuning rate. At resonance, $\Delta = 0$, and the vacuum Rabi splitting is given by

$$\Omega_R = \sqrt{4Ng_0^2 - \frac{(\Gamma_e - \Gamma_p)^2}{4}} \tag{6}$$

which shows that there is a positive correlation between Ω_R and g and the criterion of strong coupling can be obtained as

$$Ng_0^2 > \frac{\Gamma_e^2 + \Gamma_p^2}{8} \tag{7}$$

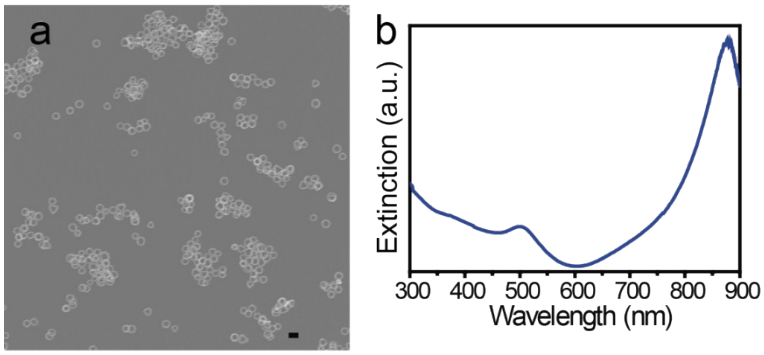

Fig. S1 (a) Large-scale SEM image of Au nanorings, demonstrating the high structural homogeneity of the Au nanorings used in this study; (b) The corresponding extinction spectrum of Au nanorings, showing two LSPR modes which appeared at ca. 500 nm (dipole out-of-plane mode) and at ca. 880 nm (dipole in-plane mode), respectively. Scale bar: 100 nm.

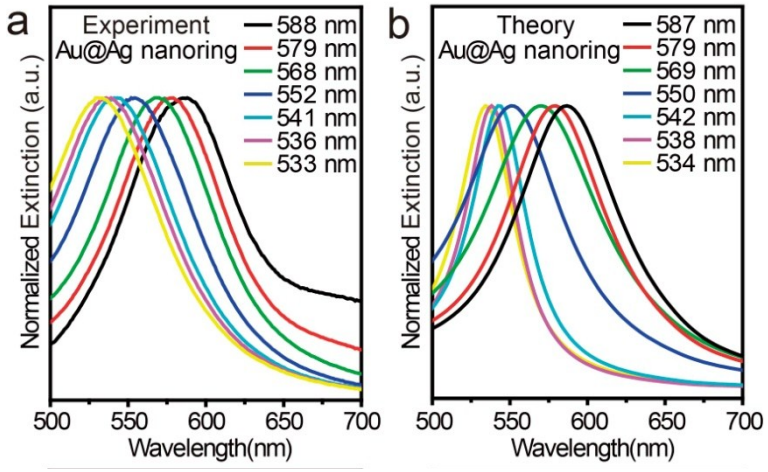

Fig. S2 (a) Experimental and (b) theoretical normalized extinction spectra of Au@Ag nanorings with different Ag shell thickness.

The plasmon resonance wavelength of Au nanorings was tuned by coating Ag shell of varying thickness. The variation in Ag shell thickness allowed for the plasmon resonance to be tuned from 588 nm to 533 nm, crossing the J-aggregate exciton resonance. FDTD method was used to calculate the optical properties of Au@Ag nanorings with varied Ag thickness (shown in Fig. S2b). Calculated spectra were in good agreement with the experimental spectra (Fig. S2a).

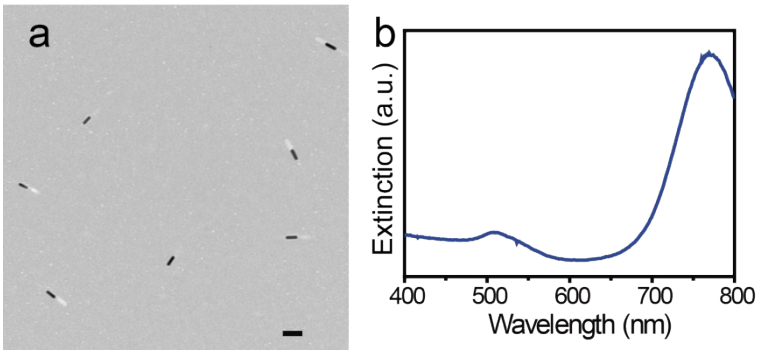

Fig. S3 (a) Large-scale TEM image of Au nanorods, demonstrating the high structural homogeneity of the Au nanorods, showing the highly purified Au nanorods with ~60 nm in length and ~15 nm in diameter; (b) The corresponding extinction spectrum of Au nanorods. The extinction spectrum shows two LSPR modes which appeared at ca. 508 nm (transverse mode) and at ca. 769 nm (longitudinal mode), respectively. Scale bar: 100 nm.

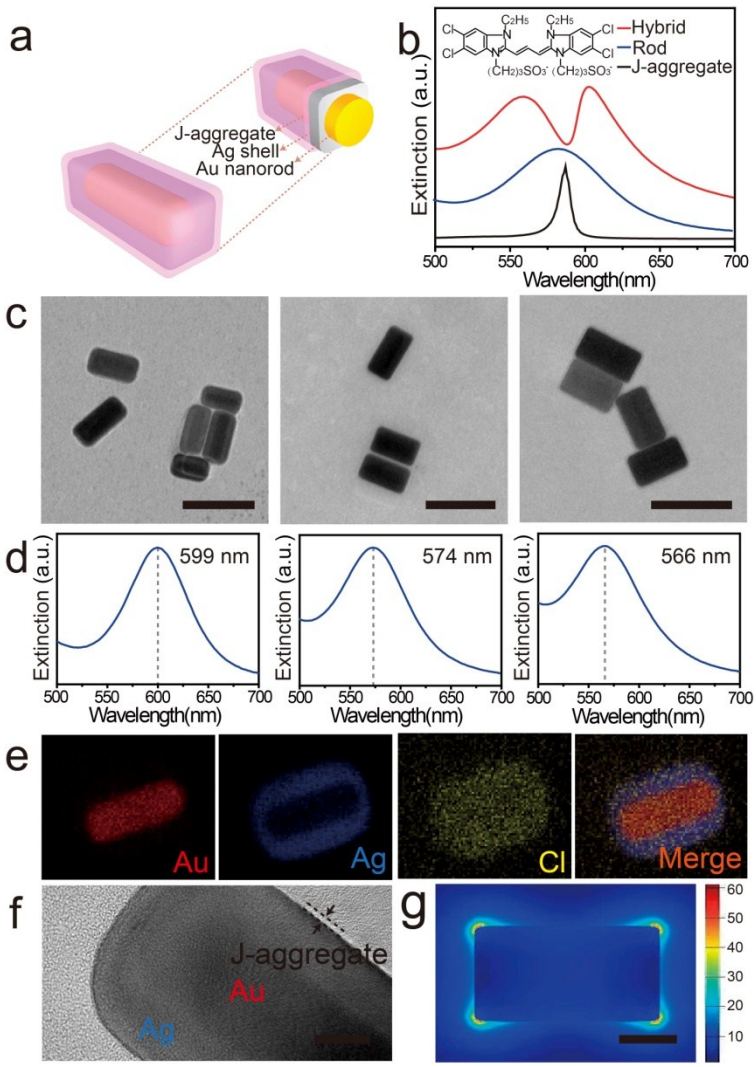

Fig. S4 (a) Schematical drawing of Au@Ag nanocuboid/J-Aggregates plexciton structure, showing a gold nanorod core and a silver shell, coated with TDBC J-aggregate; (b) Extinction spectra of free J-aggregate (black) and Au@Ag nanocuboid (blue), which upon interaction, give rise to a hybrid plexciton state (red). Inset shows the chemical structure of the molecular exciton (TDBC) used in this work; (c) TEM images of the plasmonic Au@Ag nanocuboid, coated with Ag layers of different thickness, scale bar: 20 nm; (d) The corresponding extinction spectra of Au@Ag nanocuboid above; (e) Element mapping of a single Au@Ag nanocuboid/J-aggregate; (f) HRTEM of a single Au@Ag nanocuboid/J-Aggregate hybrid, scale bar: 10 nm; (g) Electromagnetic field simulation of an individual Au@Ag nanocuboid in the x-y plane with light polarization along x-axis. Scale bar: 20 nm

The schematical drawing of the hybrid is depicted in Fig. S4a. The hybrid plexcitonic architecture contains a Au nanorod coated by a silver layer (Au@Ag nanocuboid) and encapsulated in an excitonic

matrix. The extinction spectrum of J-aggregate exhibiting a narrow peak at 586 nm (ω0=2.116 eV) was shown Fig. S4b. When Au@Ag nanocuboid supporting plasmon resonance (see Fig. S4b) matches the J-band of TDBC, a coupled hybrid system exhibits very significant mode splitting, signaling the realization of a strong coupling scenario. The plasmon resonance wavelength of Au@Ag nanocuboid was tuned by coating Ag shell of varying thickness. The silver coating process is highly controllable by the amount of Ag added. As can be seen from Fig. S4c, the final wall of Au@Ag nanocuboid gradually becomes thicker with increasing Ag amount added. The surface plasmon resonance (SPR) frequency of Au@Ag nanocuboid gradually changes from 599 to 566 nm as increasing Ag shell thickness, which is shown in Fig. S4d and Fig. S5. High resolution transmission electron microscopy (HRTEM) image of a single Au@Ag nanocuboid/J-aggregate hybrid is shown in Fig. S4f. From Fig. S4f, we can observe three layers in the structure. Since Au and Ag exhibit comparable values of lattice constants, the grain boundary was hard to be distinguished. The outer amorphous layer represents the J-aggregates layer. Elemental mapping of a single hybrid which is shown in Fig. S4e also demonstrates the different components. It was observed that the Au region is smaller than that of Ag and J-aggregate, indicating the encapsulation of silver and J-aggregate shell on Au@Ag nanocuboid. A composite of the color-coded results for Au, Ag and the J-aggregates is presented in Fig. S4e, which demonstrates elemental distribution of a single Au@Ag nanocuboid/J-aggregate hybrid. It clearly illustrates that TDBC J-aggregate form a dispersive layer around the center Au@Ag nanocuboid. The FDTD simulations of the LSP electric field enhancement in the x-y plane with light polarization along x-axis for a Au@Ag nanocuboid is shown in Fig. S4g. The LSP resonance of Au@Ag nanocuboid was tuned to the same wavelength of J band (λ=586 nm). It seems that the electric field of nanocuboid is more localized and less dissipated than ring's.

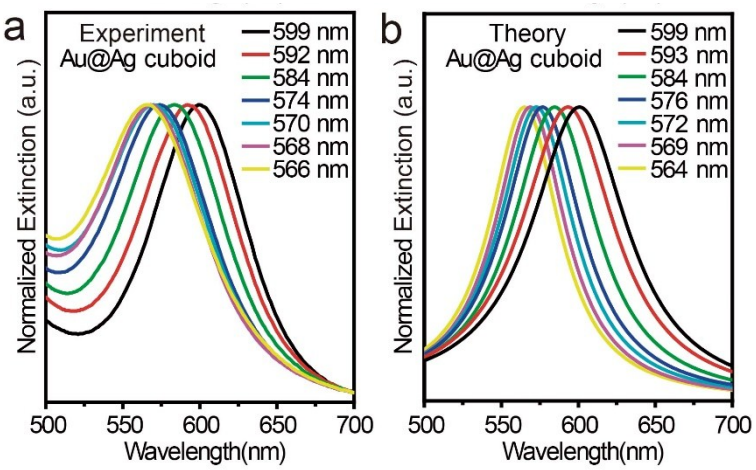

Fig. S5 (a) Experimental and (b) theoretical normalized extinction spectra of Au@Ag nanocuboids with different Ag shell thickness.

The plasmon resonance wavelength of Au@Ag nanocuboids was tuned by coating Ag shell of varying thickness. The variation in Ag shell thickness allowed for the plasmon resonance to be tuned from 599 nm to 566 nm, crossing the J-aggregate exciton resonance. FDTD method was used to calculate the optical properties of Au@Ag nanocuboids with varied Ag thickness (shown in Fig. S5b). Calculated spectra were in good agreement with the experimental spectra in Fig. S5a.

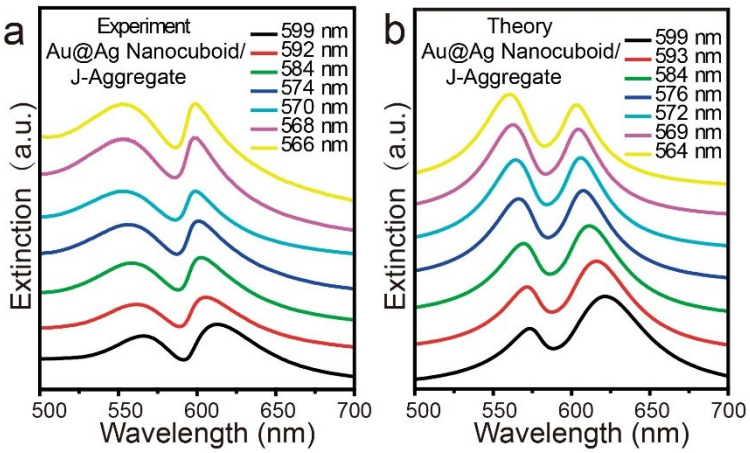

Fig. S6 (a) Typical experimental and (b) theoretical extinction spectra of the Au@Ag nanocuboids strongly coupled to J-aggregate. Each curve represents a different plasmon resonance from Au@Ag nanocuboid/J-aggregate with silver coating of different thickness. The individual curves are offset vertically for clarity.

Fig. S6a depicts the extinction properties of the Au@Ag nanocuboids/J-aggregate hybrids in solutions in which the LSPR mode is resonant with the J-aggregate transition. When the Au@Ag nanocuboids supporting LSPR modes matching the J band (~586 nm) are hybridized with the molecular aggregates, the strongly coupled hybrids exhibit significant mode splitting (~156 meV) into upper(ω+) and lower (ω-) plasmon-exciton polariton branches that are part light and part matter. Our experimental data (Fig. S6a) are accurately fitted by theoretical simulation (Fig. S6b).

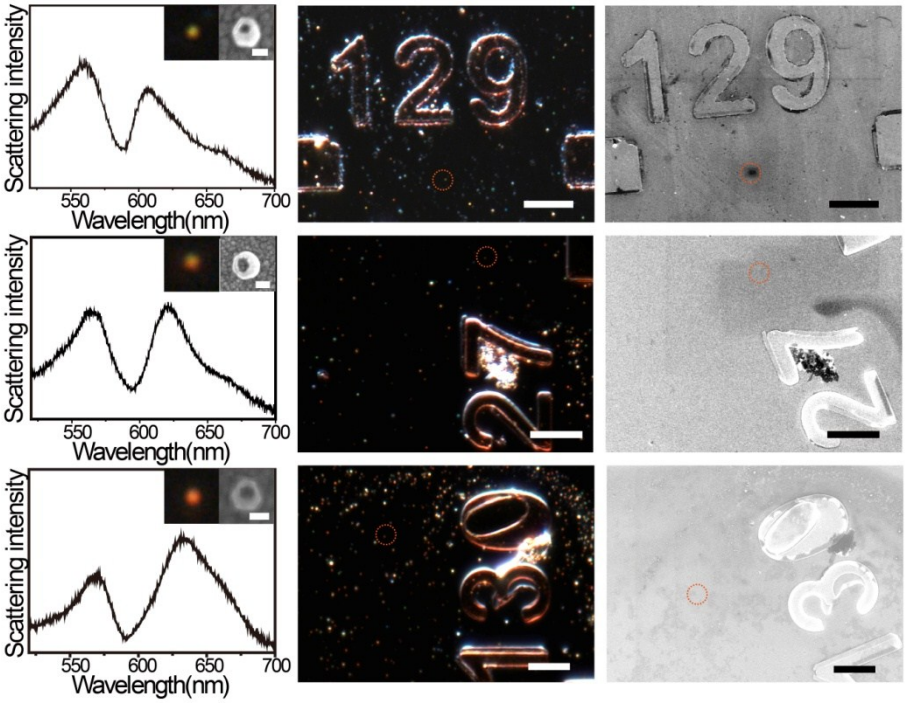

Fig. S7 (Left panel) Experimental dark-field scattering spectra of three individual Au@Ag nanoring/J-aggregate hybrids with different detunings ($\Delta<0$, $\Delta=0$, and $\Delta>0$). The insets are dark-field and SEM images of the corresponding hybrids. The spectra were taken under unpolarized white light illumination. Scale bar: 50 nm; The dark field images (Middle panel) and the corresponding SEM images (Right panel) of the same area showing the positions marked by orange circle where the particles measured in left panel. Scale bar: 10 μm.

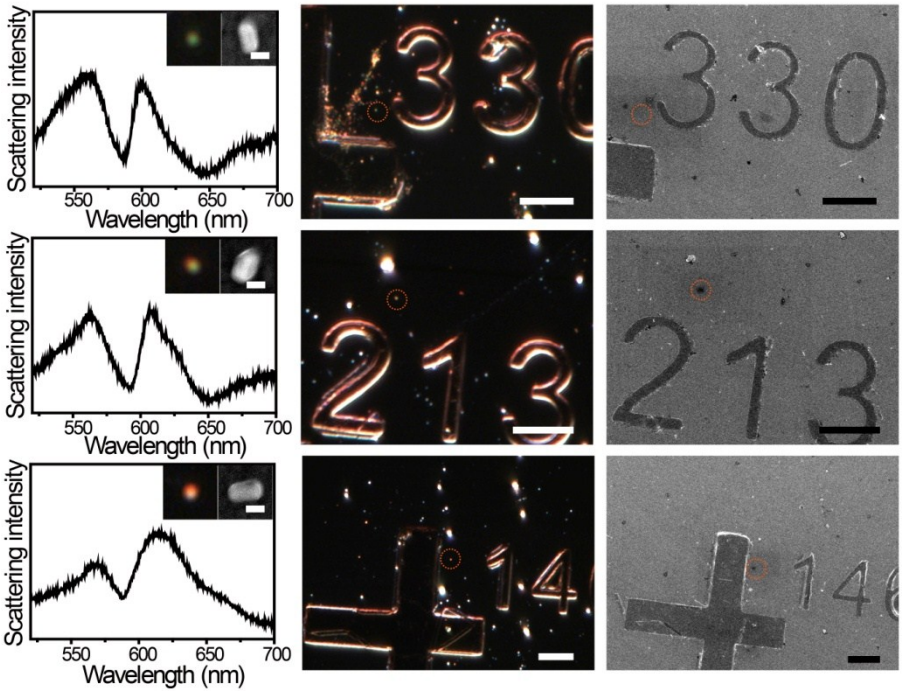

Fig. S8 (Left panel) Experimental dark-field scattering spectra of three individual Au@Ag nanocuboid/J-aggregate hybrids with different detunings ($\Delta<0$, $\Delta=0$, and $\Delta>0$). The insets are dark-field and SEM images of the corresponding hybrids. The spectra were taken under unpolarized white light illumination. Scale bar: 20 nm; The dark field images (Middle panel) and the corresponding SEM images (Right panel) of the same area showing the positions marked by orange circle where the particles measured in left panel. Scale bar: 10 μm.

REFERENCE

1. C. M. Guvenc, F. M. Balci, S. Sarisozen, N. Polat and S. Balci, *J. Phys. Chem. C*, 2020, **124**, 8334-8340.
2. M. Wersall, J. Cuadra, T. J. Antosiewicz, S. Balci and T. Shegai, *Nano Lett.* 2017, **17**, 551-558.
3. S. Balci, B. Kucukoz, O. Balci, A. Karatay, C. Kocabas and G. Yaglioglu, *ACS Photonics*, 2016, **3**, 2010-2016.
4. S. Balci and C. Kocabas, *Opt. Lett.*, 2015, **40**, 3424-3427.
5. S. Balci, *Opt. Lett.*, 2013, **38**, 4498-4501.
6. P. B. Johnson and R. W. Christy, *Phys. Rev. B*, 1972, **6**, 4370-4379.

